Research Article | Vol. 27, No. 2 | 21 Jan 2019 | OPTICS EXPRESS 1563
Optics EXPRESS

Measurement of wavefront curvature using computer-generated holograms

M. S. Kovalev,[1] G. K. Krasin,[1,*] S. B. Odinokov,[1] A. B. Solomashenko,[1] and E. Yu. Zlokazov[1,2,3]

[1] *Bauman Moscow State Technical University, ul. Baumanskaya 2-ya, 5, Moscow, 105005, Russia*
[2] *National Research Nuclear University MEPhI, Kashirskoe highway, 31, Moscow, 115409, Russia*
[3] *ezlokazov@gmail.com*
[*] *krasin.georg@gmail.com*

Abstract: The present article is dedicated to the problem of computer-generated holograms application for measurement of optical wavefront curvature with high precision. A holographic wavefront sensor scheme based on a phase-only spatial light modulator, which is used for CGH displaying, is proposed. The presented optical scheme and processing algorithm are validated with numerical simulations and experimental modelling.

1. Introduction

Currently, lasers are widely used in almost all fields of science and technology. However, the laser itself is just a source of high quality coherent light that is used in a sophisticated optical systems. Along with laser sources, optical components that are used for transport and manipulation of laser radiation between source and aiming point determine the performance of the entire system. This problem is especially determinant when high precision optical measurements are taken, or during the physical experiments and processes that require the highest possible concentration of light energy. In such a laser systems the control and measurement of light beam parameters in crucial optical units is strongly demanded.

There are different methods to measure the light wavefront curvature exist however SHWFS (Shack–Hartmann wavefront sensor) is the most popular [1–7]. While SHWFS is attractive for application due to constructional simplicity it suffers from limited spatial resolution and accuracy, an important parameter when precision of wavefront curvature estimation is required to be less than $\lambda/10$ [8–10]. One of the successive approaches of wavefront curvature accurate measurement is based on implementation of holography principles [11–17]. Application of CGH (computer-generated hologram) [18, 19] realised with the use of SLM (spatial light modulator) in HWFS (holographic wavefront sensor) provides additional flexibility of the method [20–25].

In the present article a reflection-type phase-only SLM is used to display the digitally synthesised holographic pattern in HWFS. CGH is specially designed to form a predetermined response (e.g. correlation function), when encoded wavefront model matches the wavefront function of the beam introduced at the input of HWFS. During the measurement of unknown waveform, CGH function is being approximated using digital postprocessing of optical responses captured by arrayed photodetector (CCD, CMOS etc.) and adjusting the weight coefficients of orthogonal basis expression of CGH-embedded wavefront model. Maximisation of optical correlation response in +1 diffraction order can be used as control function in approximation algorithms.

2. Wavefront detector using CGH

The scheme of CGH implementation as wavefront curvature detector is presented on Fig. 1. Firstly a beam to be tested is collimated by an optical collimator introduced by lenses L1 and L2

#348476 https://doi.org/10.1364/OE.27.001563
Journal © 2019 Received 1 Nov 2018; revised 19 Dec 2018; accepted 21 Dec 2018; published 17 Jan 2019

Optics EXPRESS

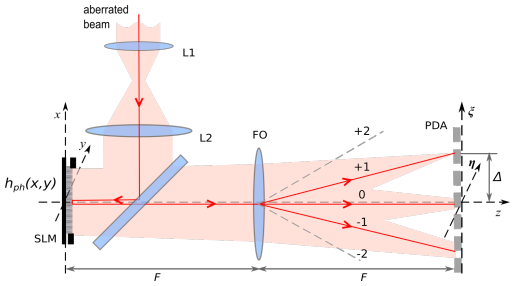

Fig. 1. Optical scheme of WFD based on reflection type phase only modulator

on Fig. 1. The parameters of collimator have to be adjusted according to input beam aperture and aperture of SLM used in the scheme. Then properly collimated beam illuminates the surface of SLM, which displays a synthesised pattern of CGH. The presented optical setup is based on reflection-type phase-only spatial light modulator that is used in combination with beam splitter to normally illuminate SLM aperture by read-out beam that has to be tested. A light beam is scattered by SLM and focused by FO (Fourier objective). PDA (photodetectors array) that is suited in back focal plane of FO acquires the output intensity distribution of light. Then the captured images are transferred for digital post-processing.

Let $f_{ref}(x, y)$ be the function of selected model of reference wavefront curvature with uniform amplitude. Function $f_{ref}(x, y)$ can be presented in the form of orthogonal serial expansion such as Zernike polynomials, Chebyshev polynomials etc., which are usual for description of aberrations. In this work we used Zernike polynomials:

$$f_{ref}(x, y) = \sum_n C_n Z_n(x, y), \tag{1}$$

where C_n are weight coefficients, $Z_n(x, y)$ are Zernike polynomials that been firstly defined in polar coordinates and then converted into Cartesian coordinates using well known definitions.

The method of CGH synthesis is based on modelling of off-axis point light source Fourier hologram record scheme with reference beam subjected to selected model of aberration distortion. According to [25] an amplitude pattern of CGH can be calculated as

$$h_{amp}(x, y) = 1 + \cos\left[2\pi\left(\frac{\Delta}{\lambda F}x - f_{ref}(x, y)\right)\right]. \tag{2}$$

where λ is wavelength, F is the focal length of FO, Δ is point light source shift from optical axis in front focal plane of FO, d_0 – CGH pixel pitch. Example of synthesised CGH structure can be seen on Fig. 2(d).

A phase-only SLM displays amplitude image as pure phase element with optical phase transparency being spatially modulated by amplitude function of the source image. Ignoring the discrete nature of SLM, applying Jacobi-Anger equation and excepting the constant phase factor, the complex amplitude continuous function of phase-only CGH synthesised according to Eq. (2) can be presented by means of first order Bessel functions $J_n(z)$ as

$$h_{ph}(x, y) = \exp\left[i\pi h_{amp}(x, y)\right] = \sum_{n\in\mathbb{Z}} i^n J_n(\pi) r_n^*(x, y) \exp\left[i\frac{2\pi}{\lambda F}n\Delta x\right], \tag{3}$$

where

$$r_n(x, y) = \exp\left[i2\pi n f_{ref}(x, y)\right] \tag{4}$$

Optics EXPRESS

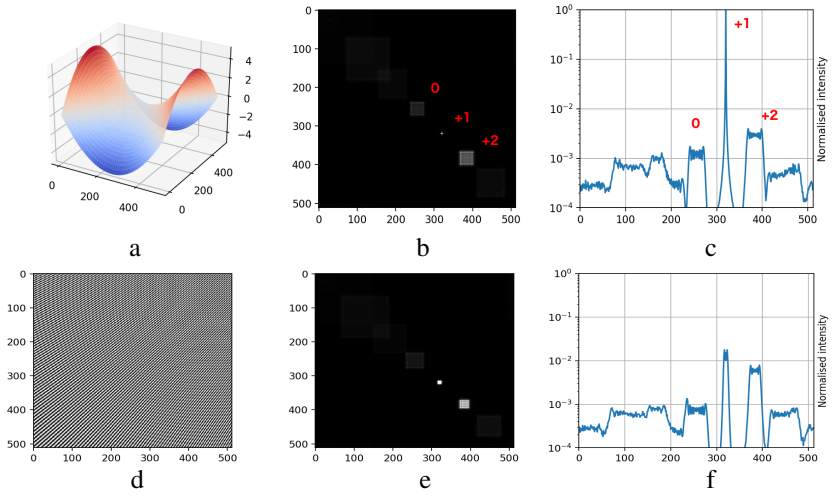

Fig. 2. The model of astigmatism with curvature depth of 10λ (a); numeric result of output light field intensity calculation and thresholding for the case when read-out beam curvature coincident to the model curvature $t(x, y) = f_{ref}(x, y)$ (b); profile function of output light field from Fig. 2(b) in logarithmic scale (c); CGH of wavefront model from Fig. 2 (d); numeric result of output light field intensity calculation and thresholding for the case $\partial\lambda/\lambda$ = 2.5 (e); profile function of output light field from Fig. 2(e) in logarithmic scale (f)

is a collection of waveforms, which phase is modulated by integer times aberration model function: $\phi(x, y) = nf_{ref}(x, y)$.

On the plane (x, y) a complex function of input beam multiplies on CGH transparency function $h_{ph}(x, y)$. Let $t(x, y)$ be the function of test beam complex amplitude. According to lens property [26], the complex amplitude of light beam at the output plane (ξ, η) can be described by means of optical Fourier transformation of light complex amplitude function in the plane (x, y), which is $h_{ph}(x, y)t(x, y)$. Assuming this, using Eq. (3), combining exponential power terms and implementing the cross-correlation theorem the output field of a system from Fig. (1) can be found as:

$$O(\xi,\eta) = \sum_{n\in\mathbb{Z}} i^n J_n(\pi) \iint t(x,y) r_n^*(x,y) \exp\left[-i\frac{2\pi}{\lambda F}\left((\xi - n\Delta)x + \eta y\right)\right] dxdy = \sum_{n\in\mathbb{Z}} i^n J_n(\pi)\left[R_n(\xi - n\Delta, \eta) \otimes T(\xi - n\Delta, \eta)\right], \quad (5)$$

where $R_n(\xi, \eta)$ and $T(\xi, \eta)$ are Fourier transformations of $r_n(x, y)$ and $t(x, y)$, $\otimes$ — a sign of cross-correlation operation.

Thus the output field contains the set of diffraction orders with the images of correlation function between input function and waveform functions from Eq. (4) spatially shifted to the value of $n\Delta$ from the optical axis. If $t(x, y) = r_1(x, y)$, the correlation term in Eq. (5) becomes the autocorrelation of pure complex phase function, and sharp thin peak appears shifted to the value Δ along axis ξ in the output field.

On Fig. 2 the results of CGH numeric modelling are presented. Figs. 2(b) and 2(c) illustrate the case when the model of read-out beam curvature is equal to the model embedded in CGH $t(x, y) = f_{ref}(x, y)$. The sharp and thin correlation peak can be found on +1 order. Figs. 2(e) and 2(f) show the case when read-out beam has 25% offset of curvature coefficient $t(x, y) = 1.25 f_{ref}(x, y)$. The correlation peak intensity in this case becomes significantly lower.

Optics EXPRESS

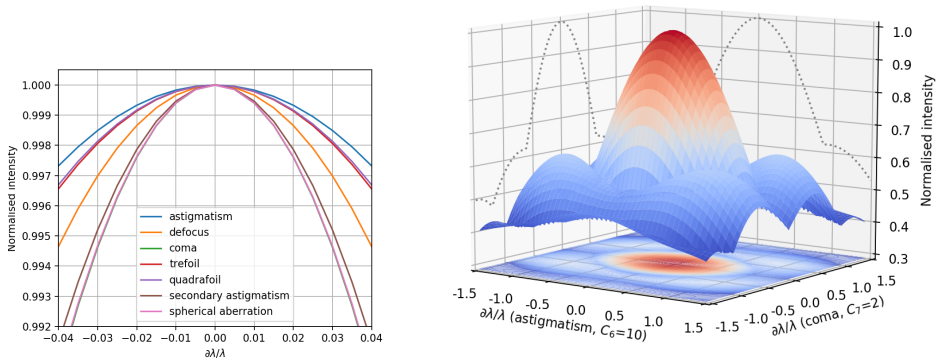

a b

Fig. 3. Dependence of correlation intensity maximum from curvature coefficient offset: for the different basis functions used in the model (a); for the case when "astigmatism" and "coma" aberrations are combined in the model (b).

On Fig. 3(a) one can see that sensitivity of $\sim 0.01\lambda$ can be achieved if optical system is capable to provide the resolution of about 13 effective bits or 76 dB of dynamical range for the worst case of astigmatism model. This can be achieved by the use of high sensitivity photodetector array and multiple exposure technique etc.

3. Processing algorithm

The measurement of aberrations is intended to be carried out using approximation of CGH embedded curvature model function (Eq. (1)) by observing output correlation signal in +1 diffraction order and recalculating CGH structure displayed by SLM in the scheme. On the first step, a rough estimation of major terms coefficients weights in Eq. (1) have to be provided using direct search method by varying the weights values in predetermined range with established rough step. A width of the peak can be used as metric for this case. Higher order terms (e.g. ±2, ±3, ...) can be used to minimise the processing time on this step. Figure 3(b) illustrates the result of numeric simulation of correlation peak intensity variation in dependance from curvature offset changes when two types of aberrations (astigmatism – 10λ and coma – 2λ) are used in the model. The values of both terms were changed in the range of $\pm 1.5\lambda$. It can be seen that in the range of $\pm 0.5\lambda$ the surface has exact extremum right in the point where offsets for both aberrations equal to zero. This indicates that further fine tuning of expansion coefficients can be provided using gradient decay method.

Correlation peak intensity is not the only metric to measure correlation response. Normalised values such as PCE (peak-to-correlation energy) and PSR (peak-to-sidelobe ratio) [27] are more attractive due to consideration not only the value of peak maximum but also sharpness of its form. In opposite to straight intensity measurement, these values are independent to laser output power fluctuation. In the present research we used PSR that can be calculated according to:

$$PSR = \frac{O(\Delta, 0) - M}{\sigma}, \tag{6}$$

where $O(\Delta, 0)$ is the value of peak amplitude, M is mean value of correlation field in the area around the peak excluding small region centred at the peak, σ is standard deviation of correlation field value in the same area where M was calculated.

Optics EXPRESS

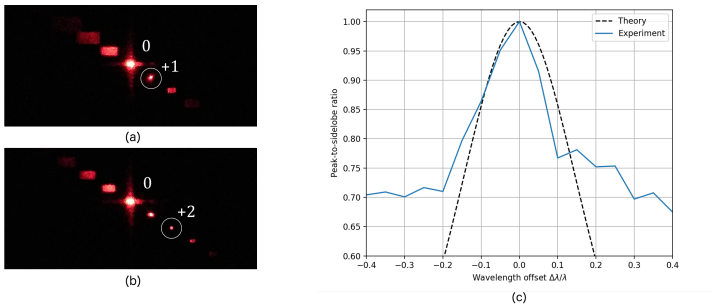

Fig. 4. Reconstructed images for 6λ defocused input light beam and CGHs with encoded defocused aberration model with curvature depth value of 6λ (a), 3λ (b), PCE value in dependance of curvature offset (c).

4. Experimental modelling of CGH-based HWFS

To validate the proposed method an experimental optical scheme of CGH-based HWFS was assembled. The experimental setup consisted of a He–Ne laser with wavelength of 632.8 nm, a phase only reflection type SLM PLUTO VIS with a 1920 x 1080 resolution, 8 μm pixel pitch, and a fill factor of 87%, and a Fourier lens with a focal length of 250 mm. Laser light beam was collimated using standard 2-lens collimator with diaphragm. High resolution digital video camera BR-5100LC-U was used to capture the output light intensity two-dimensional signals. Spatial resolution of camera is up to 2592x1944 pixels, pitch is 2.2x2.2 μm. Sensor resolution is up to 12 bits. The camera was connected to personal computer where all the postprocessing procedures were provided.

Experiments were provided with defocusing aberration. We shifted one of the collimator lenses along the optical axis in order to simulate defocusing. Firstly we adjusted the wavefront curvature using conventional SHWFS model WFS300-14AR. The value of C_4=6 was selected assuming that curvature depth of wavefront is 6λ. The same value of curvature depth and additionally 3λ was used in the wavefront model to be encoded onto CGH. Figure 4 illustrates the examples of captured light intensity distributions in the output plane of the scheme obtained during these tests. In the case of 6λ one can see the appearance of correlation peak in the 1st diffraction order. In the case when weight coefficient of the model was equal 3 ($n = 2$) a peak appears in the 2nd diffraction order. This result satisfies the effect predicted by the numeric model.

Figure 4(c) demonstrates the result of PCE calculation using setup output signal for values of curvature coefficient offset in the range of $-0.4 \leq \partial\lambda/\lambda \leq 0.4$. It could be seen that offset value of 0.05 causes the decrease of PCE to about 5% of its maximum, which is achieved in the point of zero offset. A dotted curve in Fig. 4(c) demonstrates the theoretic modelling of PSR value. It is noticeable that for small curvature offsets experimental results are in good contribution with theoretical estimations.

5. Conclusion

The present article was dedicated to light beam field aberration analysis using CGH displayed in the scheme of HWFS by phase-only SLM. Numeric simulations of the method showed that if phase-only SLM is used the higher diffraction orders can be implemented for primary rough estimation of curvature depth coefficient. Further fine estimation of curvature depth coefficient can be provided using gradient decay algorithms aimed on maximisation of correlation response. However dynamical range of about 76 dB is required for sensitivity of 0.01λ. Experimental realisation of HWFS based on CGH realised using phase-only SLM confirmed the results of numeric modelling. The sensitivity of $\lambda/20$ was observed during the experiments with

Optics EXPRESS

defocusing.

Funding

Ministry of Education and Science of the Russian Federation (Minobrnauka) (RFMEFI57717X0258), contract No. 14.577.21.0258.

References

1. V. Laude, S. Olivier, C. Dirson, and J.-P. Huignard, "Hartmann wave-front scanner," Opt. Lett., **24**, 1796-1798 (1999).
2. B. Platt and R. Shack, "History and principles of Shack-Hartmann wavefront sensing," J. Refract. Surg., **17**, S573-S577 (2001).
3. B. Pathak and B. R. Boruah, "Improvement in error propagation in the Shack–Hartmann-type zonal wavefront sensors," J. Opt. Soc. Am. **A 34**, 2194-2202 (2017).
4. J. Ko and C. C. Davis, "Comparison of the plenoptic sensor and the Shack–Hartmann sensor," Appl. Opt. **56**, 3689-3698 (2017).
5. F. Xia, D. Sinefeld, B. Li, and C. Xu, "Two-photon Shack–Hartmann wavefront sensor," Opt. Lett. **42**, 1141-1144 (2017).
6. Z. Li and X. Li, "Fundamental performance of transverse wind estimator from Shack-Hartmann wave-front sensor measurements," Opt. Express **26**, 11859-11876 (2018).
7. B. Dong and M. J. Booth, "Wavefront control in adaptive microscopy using Shack-Hartmann sensors with arbitrarily shaped pupils," Opt. Express **26**, 1655-1669 (2018).
8. P. M. Palomo, A. Zepp, and S. Gladysz, "Characterization of the digital holographic wavefront sensor," Proc. SPIE **9242**, 92421T (2014).
9. A. G. Poleshchuk, A. G. Sedukhin, V. I. Trunov, and V. G. Maksimov, "Hartmann wavefront sensor based on multielement amplitude masks with apodized apertures," Comput. Opt. **38**(4), 695–703 (2014).
10. S. Konwar and B. R. Boruah, "Estimation of inter-modal cross talk in a modal wavefront sensor," OSA Continuum, **1**, 78-91 (2018).
11. G. Andersen, F. Ghebremichael, and K. Gurley, "Holographic Wavefront Sensor – Fast Sensing, No Computing," Proc. SPIE, **6488**, 64880I (2007).
12. G. Andersen, L. Dussan, F. Ghebremichael, and K. Chen, "Holographic wavefront sensor," Opt. Eng., **48**, 085801 (2009).
13. S. Dong, T. Haist, W. Osten, T. Ruppel, and O. Sawodny, "Response analysis of holography-based modal wavefront sensor," Appl. Opt., **51**, 1318-1327 (2012).
14. A. Zepp, S. Gładysz, and K. Stein, "Holographic wavefront sensor for fast defocus measurement," Adv. Opt. Technol., **2**(5-6), 433–437 (2013).
15. P. M. Palomo, A. Zepp, and S. Gładysz, "Digital holographic wavefront sensor," Imaging Appl. Opt., OSA Technical Digest, AOT2D.1 (2015).
16. E. Anzuola, A. Zepp, S. Gładysz, and K. Stein, "Holographic wavefront sensor based on Karhunen-Loève decomposition," Proc. SPIE, **9979**, 99790X (2016).
17. F. Kong and A. Lambert, "Improvements to the modal holographic wavefront sensor," Appl. Opt., **55**, 3615-3625 (2016).
18. W. J. Dallas, "Computer-generated holograms," in *The Computer in Optical Research,* B. R. Frieden, ed. (Springer, 2005), pp. 291-366.
19. W. J. Dallas, "Computer-generated holograms," in *Digital Holography and Three-Dimensional Display,* T.-C. Poon, ed. (Springer, 2006), pp. 1-49.
20. S. K. Mishra, R. Bhatt, D. Mohan, A. K. Gupta, and A. Sharma, "Differential modal Zernike wavefront sensor employing a computer-generated hologram: a proposal," Appl. Opt., **48**, 6458-6465 (2009).
21. B. Kodatskiy, M. Kovalev, P. Malinina, S. Odinokov, M. Soloviev, and V. Venediktov, "Fourier holography in holographic optical sensors," Proc. SPIE, **10002**, 100020K (2016).
22. A. Gorelaya, M. Kovalev, P. Malinina, S. Odinokov, M. Soloviev, A. Sevryugin, and V. Venediktov, "Advanced holographic wavefront sensor," Proc. SPIE, **10233**, 102330Z (2017).
23. V. I. Bobrinev, M. L. Galkin, M. S. Kovalev, P. I. Malinina, and S. B. Odinokov, "Investigation of computer-generated Fresnel holograms for wavefront sensors," Optoelectronics, Instrumentation Data Process. **54**(1), 26–31 (2018).
24. M. S. Kovalev, G. K. Krasin, S. B. Odinokov, A. B. Solomashenko, and V. Y. Venediktov, "Hologram filters in adaptive optics problems," 2018 International Conference of Laser Optics (ICLO), St. Petersburg (2018).
25. G. K. Krasin, D. S. Lushnikov, S. B. Odinokov, A. B. Solomashenko, V. Yu. Venediktov, and E. Yu. Zlokazov, "Wavefront sensor with hologram filters in the problem of measuring phase distortions of laser radiation," Proc. SPIE, **10787**, 107870D (2018).
26. J. W. Goodman, *Introduction to Fourier Optics* (Englewood Colorado: Roberts & Co, 2005).
27. B. Kumar, A. Mahalanobis, and R. Juday, *Correlation Pattern Recognition* (Cambridge University, 2015).